Energy Performance of Four Prototypes of PVT Collectors.
A Comparative Study

Raquel Simón-Allué, Adriana Coca-Ortegón, Yolanda Lara and Isabel Guedea

[1] ENDEF Solar Solutions, Zaragoza (Spain)

Abstract

This work focuses on the energy evaluation of different liquid-based PVT collectors, with the view to obtain a PVT collector able to operate at high temperatures (above 50ºC) with acceptable thermal efficiency. To that end, the use of semi-transparent PV laminates is explored. Four prototypes were developed, tested and evaluated in controlled environment: two models with conventional silicon photovoltaic laminate and two models using a semitransparent photovoltaic laminate. Results show that the glazed PVT with frontal cover models offer better overall energy performance for STC conditions and maintain acceptable thermal efficiencies (30% and 45% depending on the PV laminate) when working at temperatures above 50ºC. Prototypes without frontal cover show good thermal efficiency at STC but present a strong dependency with the operational temperature and wind velocity. Semi-transparent PV laminate remains as an interesting possibility when the PVT collector must operate at high temperature but the electricity production is reduced, still needs to improve the ratio between electricity and thermal energy.

Keywords: PVT; glazed, unglazed, transparent laminate, experimental performance.

1. Introduction

Photovoltaic-thermal (PVT) collectors combine in a single panel, electricity and thermal energy production. PVT collectors usually have a frontal photovoltaic laminate with a rear absorber or heat exchanger (HX), through which thermal energy is extracted at low temperatures. Main classifications are performed based on the heat transfer fluid used (mainly liquid-based, air-based and refrigerant-based); type of solar input (concentrated, flat plate, parabolic, etc.); type of PV technology (mono-Si, poly-Si, other PV tech) and thermal absorber designs (copper sheet and tube, aluminum roll bond, polymeric box) (Herez et al., 2020; Joshi and Dhoble, 2018; Sultan and Ervina Efzan, 2018; Wu et al., 2017). In general, compared to the PV technology, PVT collectors get better overall energy efficiency (electrical and thermal) by unit area, therefore this technology is gaining interest for the development and implementation of net zero and positive energy buildings.

The most extended PVT type used is the liquid-based PVT collector, which represents 59% of the total area installed in the existing PVT system (Baggenstos et al., 2020). Solar technologies, PVT included, have grown in the global market significantly during the past 5 years, as shown in recent reports by the International Energy Agency (IEA). Specifically, PVT technology is growing in the European and Asian markets, dedicated mostly to domestic hot water production (IEA-SHC, 2022). Their potential was also highlighted by the IEA through the Task 60 (IEA-SHC, 2018), dedicated exclusively to the PVT systems and applications.

This technology may be used for diverse applications, such as pool heating, domestic hot water production, heating space, solar drying, and heat production for processes at low temperatures. However, the temperature requirements of the final application also determine the most suitable PVT collector type for each case. The higher temperature production, the lower thermal efficiency is finally obtained from the PVT collectors. Also, depending on climatic conditions the production temperature is limited according to the thermal behavior.

Thermal insulation level is a key factor that directly affects the energy performance of the PVT collector in both the thermal and electrical contribution. Depending on the insulation level there are two main types of liquid-based PVT collectors: *Unglazed PVTs*, with rear insulation layer but the PV module directly in contact to the environment; and *Glazed PVTs,* with an additional glass cover on the frontal face to limit thermal losses and to improve the thermal production of the PVT collector.

The purpose of this work is to study the performance of different PVT prototypes capable of working with good thermal efficiency even at high temperatures. The objective is to obtain a PVT collector suitable for applications

where electricity and hot water above 50-55ºC are required. To that end, we explored the possibility of increasing the incident solar radiation on the thermal absorber by using a semi-transparent PV laminate. Thus, four different prototypes were defined, developed, and tested in the frame of the European H2020 MiniStor project. The testing procedure was performed under steady state conditions, following the requirements of the UNE-EN-ISO 9806 (ISO 9806, 2017). Thermal and electrical performance were compared between prototypes at different operating temperatures.

2. PVT Prototypes Description and Methodology

2.1 MiniStor Project background

The research presented in this paper was developed in the context of H2020 European Project, MiniStor (Minimal Size Thermal and Electrical Energy Storage System for In-Situ Residential Installation), which focuses on the design of a novel compact integrated thermal storage system for achieving sustainable heating, cooling and electricity storage that can be adapted to existing systems in residential buildings. This system is based on a Thermochemical (TCM) reactor combined with hot and cold phase-change materials (PCM), and in parallel with an electrical storage system based on Li-ion batteries. The MiniStor system can be activated by different Renewable Energy Sources (RES), such as hybrid Photovoltaic-Thermal (PVT) collectors, Flat-Plate solar thermal Collectors (FPC), biomass and other local RES.

The TCM storage system requires temperatures above 50°C to start the corresponding reactions and storage of the heat produced by the RES. One of the goals of MiniStor project was the design a solar system using PVT subsystem to produce heat for the activation of the TCM with suitable overall energy efficiency (electrical and thermal); in this line, several PVT prototypes were developed, tested and included in several simulations of the overall system. This paper presents the main results obtained for four PVT prototypes developed and tested during the MiniStor project. Most promising prototypes were considered for its integration with the TCM storage system. More information about this integration (between solar subsystem and general system) and the whole storage system under development in MiniStor project can be found in Zisopoulos et al., 2021.

2.2 PVT prototypes description

Four PVT models were designed, developed and tested in a controlled environment. Prototypes 1 and 2 are based on conventional silicon PV laminates, while prototypes 3 and 4 use a semi-transparent PV laminate, so the incident solar radiation can pass directly onto the thermal absorber. At the same time, thanks to the PV laminate cells, it is also possible the simultaneous production of electricity. Figure 1 shows the corresponding layer configuration used in each one, while Tab. 1 gathers the main technical characteristics.
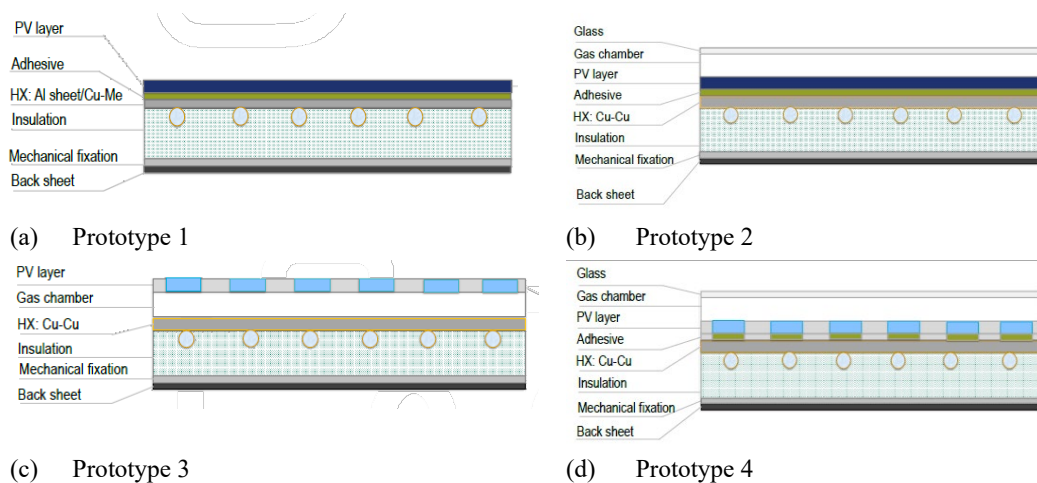

(a) Prototype 1
(b) Prototype 2
(c) Prototype 3
(d) Prototype 4

Figure 1: Sectional view of the different PVT tested prototypes.

Tab. 1:Technical characteristics of PVT prototypes.

	Prot. 1	Prot. 2	Prot. 3	Prot. 4
External configuration	Unglazed	Glazed	Unglazed	Glazed
Gross area [m²]	1.7	1.63	1.62	1.62
Aperture area [m²]	1.64	1.58	0.89	0.89
Absorber area [m²]	1.31	1.53	1.53	1.53
PV technology	Mono - Si	Poly - Si	Semitransparent Poly - Si	Semitransparent Poly - Si
Peak power [W]	320	270	160	160
Nominal efficiency [%]	18.8	16.6	9.91	9.91
V_{mpp} [V] - I_{mpp} [A]*	33.4 / 9.58	31.19 / 8.67	19.05 / 8.43	19.05 / 8.43
Temperature coefficient of voltage / current [%/K]	- 0.29 / 0.05	-0.30 / 0.038	-0.345 / 0.046	-0.345 / 0.046
Absorber material	Copper + aluminium	Copper	Copper	Copper
Absorber geometry	Sheet & tubes (meander)	Sheet & tube (harp)	Sheet & tube (harp)	Sheet & tube (harp)
Tested flow [l/h]	85	125	125	125

* Measured at Standard Testing Conditions (STC): 1000W/m2; cell temperature at 25ºC; AM1.5.

Prototype 1 is an unglazed PVT collector. It has a PV laminate with a gross area of 1.7 m², made of monocrystalline silicon cells (peak power of 320 W). The thermal absorber design is Sheet & Tube type absorber made of an aluminum sheet with copper tubes in a meander arrangement (Figure 1.a). The integration between the PV layer and the thermal absorber was performed by using mechanical methods and an adhesive acrylic type. Finally, the rear enclosure was added with a 30 mm thick rock-wool insulation layer.

Prototype 2 is a glazed PVT collector, with a PV laminate with a gross area of 1.63 m² made of polycrystalline silicon cells (peak power of 270 Wp). The thermal absorber design is Sheet & Tube made with a copper sheet and copper tubes arranged in harp (Figure 1.b). The integration between the PV layer and the thermal absorber was performed also using mechanical methods combined with an adhesive acrylic type. This prototype has a frontal transparent insulation cover, composed of a 3.2mm glass and a gas chamber, as well as a rock wool rear insulation layer.

Prototype 3 is an unglazed PVT collector that uses a semi-transparent PV laminate with a gross area of 1.62 m². The silicon cells cover only 54% of their gross surface transparent, so the nominal electrical power is lower, with a value of 160 Wp. This prototype uses the same type of thermal absorber as prototype 2, but the PV laminate is not in direct contact with the copper sheet since there is an internal air camera between both components. As a result, the solar incident radiation arrives at the thermal absorber (Figure 1.c).

Prototype 4 is a glazed PVT collector that has the same components of Prototype 3 (semi-transparent PV laminate and copper absorber) but the air camera is located on the frontal face of the collector. Thus, the frontal cover implies frontal insulation as introduced in Prototype 2, as well as a rock wool rear insulation layer (Figure 1.d).

In all cases, PV layer includes also several sub-layers in all prototypes: the first is a protective photovoltaic glass, followed by the silicon cells, encapsulated in EVA, and finally a back sheet.

2.3 Testing methodology

The testing procedure were carried out according to EN-ISO 9806 standard (ISO 9806, 2017), following the static testing methodology. For each prototype, the tests were carried out for several days, to ensure different levels of wind severity. Experimental tests were performed under natural irradiance in Zaragoza (Spain). PVT prototypes were placed in an in-house testing rig with an inclination of 45º and were manually oriented to the sun to guarantee a constant solar irradiation during several hours each day (between 900-1000W/m2). During the testing period, panels were forced to operate in a close hydraulic loop at different inlet temperatures with the PV laminate performing at MPPT (maximum production point).

Thermal performance was obtained by using temperature sensors (PT-100), flow meter (Pulse Teko TC1) and pressure gauge (Unik 5000), while the electrical performance was evaluated by measuring the current and voltage generated in CC in the panel. Environmental data (global irradiance, ambient temperature and wind speed) were measured through a weather station composed of a pyranometer (LP Pyra 03) and a wind gauge (Thies 4.3303.22). All sensors reported data with a frequency of 1 min, which was registered in a PLC Modicon 241 for the subsequent analysis. A scheme of the testing rig and main components is shown in Figure 2, with the hydraulic (in blue), electrical (in red, CC in continuous and CA in dash line) and monitoring (in purple dash line) connections.
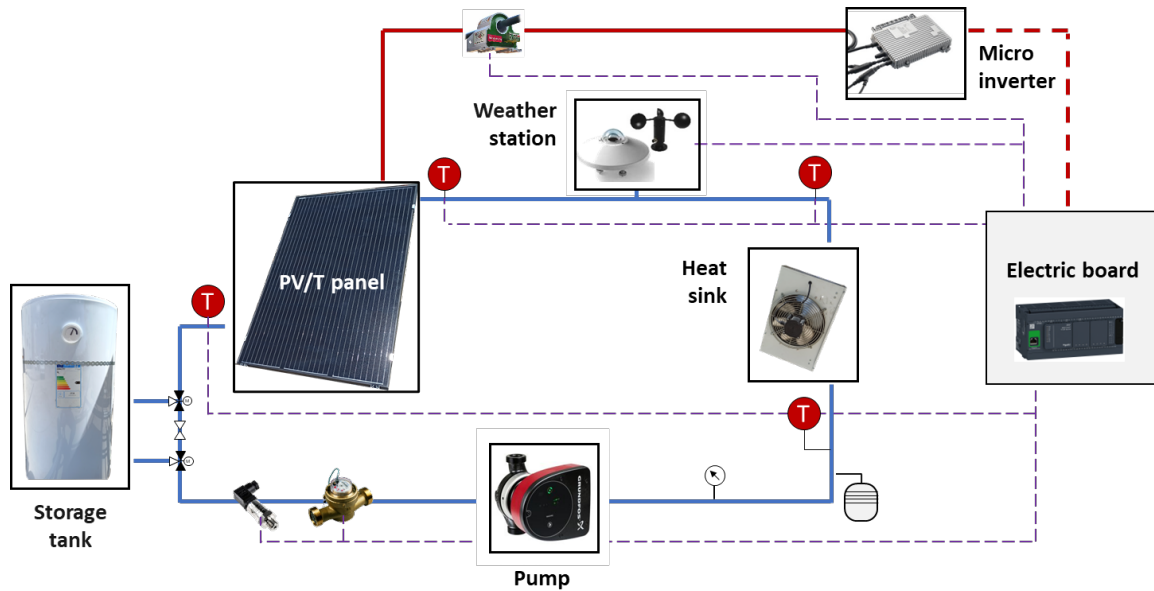

Figure 2: Flow diagram of the PVT testing rig.

2.4 Mathematical considerations

The instantaneous thermal effective power generated by each prototype is calculated after the testing procedure through the equation (eq. 1). This equation is based on the thermal gap of the fluid measured between the outlet and the inlet of the panel (ΔT), the flow rate inside the circuit ($\dot{m}$) and the specific heat of the water (c_f). Then, the instantaneous thermal efficiency was calculated through (eq. 2, considering the solar irradiance (G) and the gross area of the PVT panel (A_G).

$$\dot{Q} = \dot{m} \cdot c_f \cdot \Delta T \qquad \text{(eq. 1)}$$

$$\eta_{th} = \dot{Q} \Big/ (A_G \cdot G) \qquad \text{(eq. 2)}$$

The electrical power of each prototype was also registered during the testing, measuring the electrical current circulating through the panel (I_p) and calculated through the (eq. 3) . The voltage was estimated from the V_{mppt} value of the PV panel, considering the penalization of temperature, following the relation:

$$W_p = I_p \cdot V_p \qquad\qquad\qquad \text{(eq. 3)}$$

$$V_p = V_{mppt} \left(1 - \alpha_{PV} \left(T_c - T_{STC}\right)\right) \qquad\qquad \text{(eq. 4)}$$

Where α_{PV} is the voltage temperature coefficient of each PV laminate (indicated in Tab. 1), T_c the cell temperature and T_{STC} the cell temperature at standard test conditions (T_{STC}=25°C). The cell temperature has been estimated based on the environmental conditions (solar radiation and temperature) and the nominal operating temperature of the cell, T_{NOC}, set by the manufacture as 45°C.

Then, the instantaneous electrical efficiency was calculated by means of (eq. 5).

$$\eta_{PV} = {W_p}\big/{(A_{PV} \cdot G)} = {(I_p \cdot V_p)}\big/{(A_{PV} \cdot G)} \qquad\qquad \text{(eq. 5)}$$

2.4.1 Thermal characterization

The parameter identification of the PVT panels has been performed according to the international standard ISO 9806, corresponding to each type of collector here tested. The most updated standard, ISO 9806, 2017, indicates the obtaining of eight parameters to define the thermal performance of a collector, as well as the considerations of reduced wind speed ($u' = u - 3\,m/s$) instead of direct wind measurement and net irradiance on the collector plane. In this article, the procedure indicated in the ISO 9806, 2013 is preferred through, as has been used by other authors (Bianchini et al., 2017; Brötje et al., 2018; Jonas et al., 2019; Simón-Allué et al., 2022), since it is considered that favors the comparison between different collectors.

For steady-state collector efficiency tests, the ISO 9806, 2013 differentiates the thermal model characterization as a function of the collector type, discretizing the performance of uncovered or WISC collectors (wind and/or infrared sensitive) with a linear mathematical model and the glazed collectors with a quadratic model.

According to this standard, the thermal performance of a covered collector is characterized through the quadratic relation depicted in (eq. 6, where η_0, a_1, a_2 are the thermal performance coefficients of the collector. η_0 is the optical efficiency and represents the collector efficiency at $T_m = T_a$, while a_1 and a_2 are the linear and quadratic heat loss coefficient respectively. T_m is calculated as the average between the inlet and outlet collector temperature, calculated as stated in the standard. This formula is function of the collector operating parameter ($T_m - T_a$), mean fluid temperature and ambient temperature and G, solar irradiance.

$$\eta_{th} = \eta_0 - a_1 \left(\frac{T_m - T_a}{G}\right) - a_2 G \left(\frac{T_m - T_a}{G}\right)^2 \qquad\qquad \text{(eq. 6)}$$

The thermal performance of the uncovered or WISC model is characterized through the linear relation of (eq. 7, where η_0, b_u, b_1, b_2 are the thermal performance coefficients of the collector. In this case, η_0 is the optical efficiency, b_u is the wind dependence of collector efficiency coefficient, b_1 the linear heat loss coefficient and b_2 the wind dependence of the heat loss. The WISC model includes the dependency with u, wind speed, and G'', the net irradiance. This magnitude can be calculated following the (eq. 8, according to the ISO 9806, 2013, where α is the solar absorptance, ε is the hemispheric emittance and E_L the longwave irradiance.

$$\eta_{th} = \eta_0 \left(1 - b_u u\right) - \left(b_1 + b_2 u\right) \frac{T_m - T_a}{G''} \qquad\qquad \text{(eq. 7)}$$

$$G'' = G + \frac{\varepsilon}{\alpha} \left(E_L - T_a^4\right) \qquad\qquad \text{(eq. 8)}$$

Operational parameters T_m, T_a, G and u are directly measured during the testing procedure. Thermal performance coefficients are calculated by least-squares approximation, through curve fitting of the experimental data. Quadratic model was used for the characterization of Prot. 2, 3 and 4 and linear model was used for the characterization of Prot. 1, based on the experimental measurements.

2.4.2 Statistical analysis

An additional statistical analysis has been applied to the parameter characterization in order to assess the suitability of the model assumptions presented here and the goodness of the final fit. The strength of the relationship between thermal performance and the abscissa operational parameter $\left(\frac{T_m - T_a}{G}\right)$ has been evaluated through the calculus of the Pearson's correlation (r_{xy}) coefficient for the Prot. 1 (expected linear relation). It indicates the level of linear dependency between both variables: perfect fitting (r=1), no relation (r=0), positive dependency (r>1) or inverted dependency (r<0).

For Prots. 2 – 4, Spearman coefficient has been used instead, to determine if thermal efficiency and the abscissa operational parameter $\left(\frac{T_m - T_a}{G}\right)$ are monotonically related, even if their relationship is not linear, as it expected. The analysis of this coefficients is the same of the Pearson's one.

Besides, the goodness of the regression is assessed through the coefficient of determination R^2, calculated as indicated in (eq. 9) between the experimental measurement y_i and the numerical approach $\bar{y}$.

$$R^2 = \frac{\sum(\widehat{y_i} - \bar{y})^2}{\sum(y_i - \bar{y})^2} \qquad\qquad \text{(eq. 9)}$$

3. Results & discussion

3.1 Energy efficiency

A summary of the electrical and thermal efficiencies obtained for the four different PVT collectors is provided in Figure 2, with energy efficiency values placed in the y-axis and the operating parameter $\left(\frac{T_m - T_a}{G}\right)$ in the x-axis. Experimental data were obtained slightly displaced on the X-axis depending on the season where they were tested. Thermal efficiency is shown in blue and electrical value in red. An overall performance has been calculated considering electrical and thermal efficiency as the direct sum of both quantities, as performed in previous works (Fayaz et al., 2019; Ozgoren et al., 2013). Although the addition of two different types of energy should be taken with caution, having a single factor to compare the overall efficiency of collectors is useful.

Efficiency results indicate that Prototypes 2 and 4 (both with frontal cover) exhibited the highest values for overall performance (63.4% and 64% respectively in STC) while maintaining an acceptable thermal performance for high operation temperature (thermal efficiency around 30% and 45% respectively when working 25ºC above environment). Prototypes 1 and 3, on the contrary, showed lower thermal and overall efficiency for the whole testing range (overall efficiency: 56.5% - 46.1% respectively under STC, and 26.2% - 20.1% when working 25ºC above environment).

Regarding the electrical performance, better results were found for the unglazed model as expected, not only for the higher nominal efficiency of the PV laminate, but also for the lower operational temperature due to the absence of frontal cover.

The incorporation of semi-transparent PV laminates severely decreases the electrical production of the panel, as the PV panel has half nominal power of the PV laminated used in Prot. 1. This should provoke direct benefits on the thermal performance since more amount of solar radiation is able to reach the thermal absorber. However, according to the experimental results, this benefit is obtained when the PV laminate is direct contact to the absorber (Prot. 4) and not when an air camera separates both components (Prot. 3). No significant improvement in electrical production is found in this case when the semi-transparent PV laminate is in direct contact to the surrounding ambient (Prot. 3) versus the same configuration with the frontal cover (Prot.4), probably because refrigeration effect of the thermal absorber contributes in this last case to decrease the operational cell temperature.
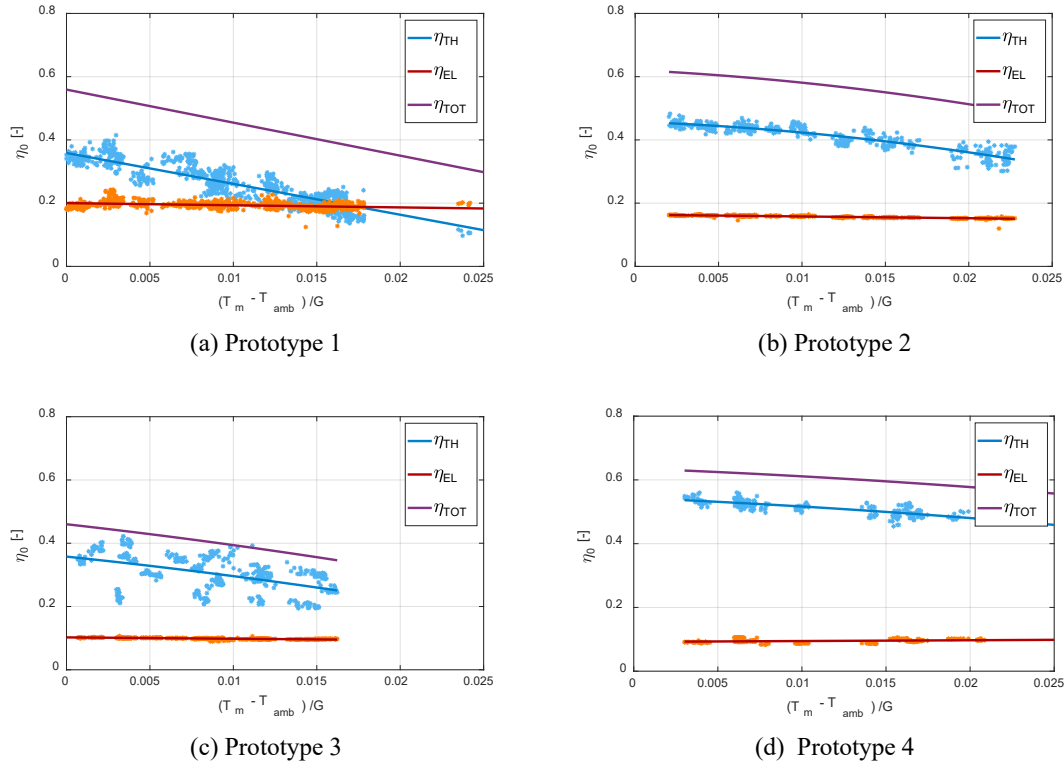
(a) Prototype 1   (b) Prototype 2

(c) Prototype 3   (d) Prototype 4

Figure 3: PVT efficiencies.

3.2 Thermal parameter characterization

The values of the thermal performance coefficients, defined as stated in the ISO 9806, 2013, are calculated for all prototypes based on the eq. 6 and eq. 7. The values obtained for each case are gathered in Tab. 2, together with technical values to assess the goodness of the adjustment.

Prototypes with frontal glazing present higher values of optical efficiency (η_0) followed by the uncovered panel (Prot. 1) and the one with rear camera (Prot. 3). For the Prot. 1, higher values of η_0 were expected due to the absence of frontal cover at low operational temperatures. An optical efficiency value below the other prototypes can be explained due to the material composition of the thermal absorber (sheet of aluminum instead of copper), the geometry (meander instead of harp configuration), lower operational flow rate or an enhanced electrical generation.

Prot. 1 also presents the higher linear heat loss coefficient (b_1) which implies that the thermal efficiency is strongly decrease when the operational temperature is increased, as it is the main purpose in this project. Glazed prototypes, on the contrary, show the lower values of heat loss coefficients, indicating that they are able to maintain acceptable efficiency levels even when the collector increases temperature. Between these two cases, it is highlighted the Prot. 4, which also presents a lower value of a_2 (quadratic term). This implies a better efficiency than Prot. 2 when the PVT panels performs at high temperature.

Tab. 2: Thermal performance coefficients and main adjustment characteristics. *Electrical efficiency value is given for Tm = Ta.

	η_0	b_u	b_1 / a_1	b_2 / a_2	η_{EL}*	N	SE	r (Pearson)	ρ (Spearman)	R^2
Prot. 1	0.380	0.0312	9.77	-0.122	0.20	911	0.0258	-0.9228	-0.9199	0.8717
Prot. 2	0.457	-	2	0.148	0.163	427	0.0160	-0.9057	-0.8803	0.8363
Prot. 3	0.358	-	5.49	0.0712	0.102	537	0.0466	-0.5989	-0.6044	0.3597
Prot. 4	0.544	-	2.25	0.00576	0.093	247	0.0145	-0.9026	-0.8398	0.8268

Tab. 2 also includes some information about the quality of the numerical adjustment obtained with the thermal coefficients. Particularly, this table shows for each prototype case: N, as the number of individual measurements, SE as the Standard Error of the regression, r as the Pearson coefficient, ρ as the Spearman coefficient and R^2 as the determinant coefficient, all of them defined in Section 2.4.2.

The value of Pearson's (**r**) and Spearman (**ρ**) coefficients reflects a negative relation, which means that the thermal efficiency decreases as the variable $\left(\frac{T_m - T_a}{G}\right)$ increases. Pearson's coefficient show a strong linear relation between variables ($-0.9 > r > -1$) for all prototypes except the Prot. 3, where a poor relation is found ($r > -0.6$). Spearman's coefficient supported this finding, demonstrating that the behaviour of Prot. 3 is not only not linear, but seems to depend on some additional variable besides the temperature gap and the solar irradiation.

3.3 Uncertainty analysis

All PVT prototypes exhibit some level of dispersion in the experimental data, as expected in measurements taken with real environmental data. However, both prototypes without frontal cover (Prot. 1 and 3) present much higher dispersion level than the prototypes with (Prot. 2 and 4), although the nature for this dispersion seems to come from different sources. To better evaluate this effect, we include in Figure 4 the histogram of errors, a graphical analysis of the error committed in the thermal efficiency when is calculated through the numerical characterization of Section 2.4.1 (η_{cal}) or experimental measurements (η_{exp}). For each case, determination coefficient R^2 is included in each subfigure, also added in Tab. 2.

For uncovered prototype case (Prot. 1, Figure 4 (a)), the range of error between theoretical and experimental thermal efficiency is wider than in other cases, however, the coefficient of determination R^2 is closer to 1, which should indicate better adjustment. This can be explained because the number of measurements taken during the testing of Prot. 1 (N=911) is much greater than those used in Prot. 2 and 4 (N=427 and N=247 respectively). As the number of items are much higher, the possibility to obtain bigger errors increases, although the general adjustment considering the whole period testing is better.

Moreover, it should be remarked that this model depends not only on the $\left(\frac{T_m - T_a}{G}\right)$ parameter, but also on the wind speed (see (eq. 6)). The theoretical model incorporates this variable, but the graphical representation of Figure 3 (a) is shown for the average wind speed measured during the testing. The dispersion found in this figure around the linear performance is then a consequence of the different wind levels registered during the testing, and not an inaccuracy of the thermal model.

The prototype with the rear camera (Prot. 3) is different. In this case the graphical dispersion shown in Figure 3 (c) is higher than any other case, as is the error range between theoretical and experimental results shown in Figure 4 (c). Moreover, the gaussian curve generated in the histogram of Prot.3 has a much flatter profile than the other three cases, which presents a sharper profile with higher frequencies located close to zero. This poor adjustment is clearly represented by the R^2 value of 0.3597 calculated for this case. This fact indicates that the thermal model considered for this prototype may not be suitable, since this theoretical model is not able to reproduce the experimental performance with enough accuracy.

Two approaches are proposed to address the adjustment to this model. First one is to include some dependency of the wind speed, since it has been noticed during the testing that this variable has some influence on the final thermal performance. As the relation with the temperature parameter $\left(\frac{T_m - T_a}{G}\right)$ has proved to be clearly quadratic, the question remains whether the relationship with wind is quadratic or linear. Second one exposes the possibility of developing a new theoretical model to characterize this particular solar panel, since none of the models presented in ISO 9806, 2013 seems to be able to predict the thermal performance due to the presence of air camera between the PV and absorber.
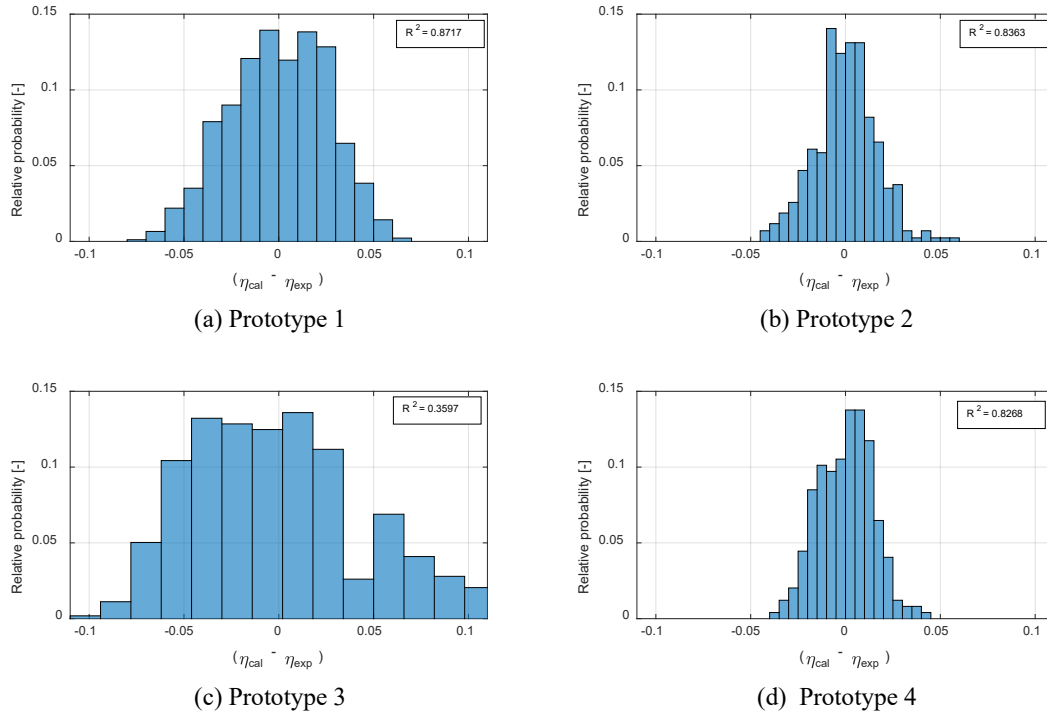
Figure 4: Histogram of error committed between theorical data (η_{cal}, calculated from linear or quadratic models) and experimental data (η_{exp}), and coefficient of determination R^2 for each adjustment.

3.4 Power production

As explained in 2.1, the objective of the project was to find a PVT panel able to work at 50ºC with still useful thermal efficiency. In order to assess the appropriateness of prototypes at the operating conditions required in end use, we have calculated the power production (thermal and electrical) of each prototype when working at mean operational temperature of 50ºC. For this comparison, STC conditions (1000W/m², Ta=25ºC, wind=1m/s) are considered. Graphical results are shown in Figure 5 while particular values for operational temperature of T_m= 50ºC are gathered in Tab. 3.

In these figures, the relation of each prototype with regard to the thermal losses is graphically shown. At STC conditions, Prot. 1 (Figure 5 (a)) presents full linear behavior with a strong negative slope, as stated by the linear coefficient (b_1=9.77). Lower thermal efficiencies are expected for higher values of wind speed. Thanks to the electrical potential of this PV laminate, the total power generated by this prototype at 50ºC is 286.5 W/m², where only 104.7 W/m² provided for thermal process.

Prot. 3 (Figure 5 (c)) presents better thermal generation but lower electrical production than Prot. 1, in a slightly smaller gross area. As a consequence, the total power production is a bit lower (270.3 W/m²), but more thermal contribution can be provided to the end user. This estimation however should be analyzed with more detail since the evaluation of the adjustment and the thermal model used cannot be considered as satisfactory.

Finally, both glazed models (Prot. 2 and 4, Figure 5 (b) and (d)) present reasonable total energy productions at 50ºC, which reached to 473.9 W/m² for the Prot. 2 and 571.5 W/m² for Prot. 4. The main difference lay in the thermal-electrical ratio obtained in each model, which was 66-34% for Prot. 2 and 84-16% for Prot. 4. Based on this data, it is concluded that both collectors are recommended for their use in the final application.
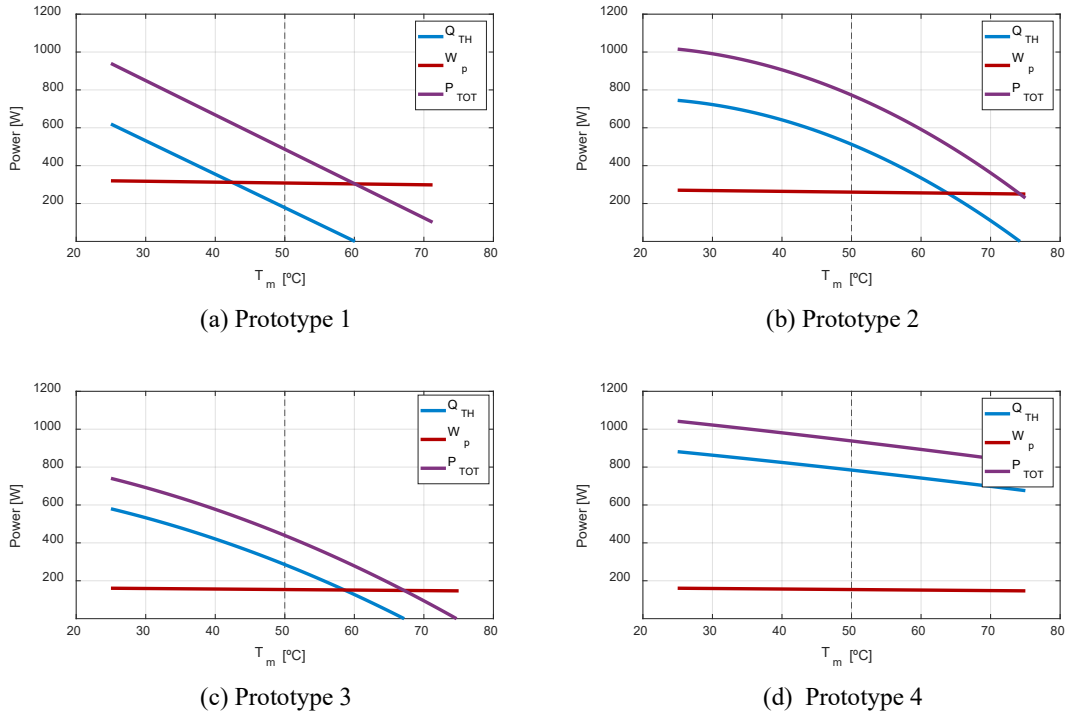
(a) Prototype 1

(b) Prototype 2

(c) Prototype 3

(d) Prototype 4

Figure 5: PVT power production at STC (1000W/m², Ta=25ºC, wind=1m/s).

Tab. 3: Estimated power production of PVT prototypes at 50ºC and STC.

	Prot. 1	Prot. 2	Prot. 3	Prot. 4
Thermal power [W]	178	512	285	784
Thermal power [W/m²]	104.7	314.1	175.9	481
Electrical power [W]	309	260.5	153.5	153.8
Electrical power [W/m²]	181.8	159.8	94.4	90.5
Total power [W/m²]	286.5	473.9	270.3	571.5

This study is not exempt form limitations. Although the analysis fulfilled its objective of selecting suitable and most promising PVT prototypes for their ulterior integration with TES system, the characterization of Prot. 3 should be improved. One possibility would be to develop a mathematical model for this particular PVT design. A second and more recommended way would be to obtain the thermal characterization through the 8-parameter equation indicated in the updated version of the standard, ISO 9806, 2017. The main future line of this study is to develop a procedure to be able to characterize the four prototypes here proposed under the last version of the standard, and compare numerical approaches.

4. Conclusions

This work presents the results of testing four liquid-based PVT prototypes considered for their future use as thermal and electricity collectors, in the frame of an electrical storage system developed under a H2020 European project. Prototypes were designed, manufactured and tested according to EN-ISO 9806 standard (CEN, CENELEC 2017).

Experimental testing and subsequent numerical analysis allowed to characterize the thermal behavior of prototypes based on the models given in the ISO 9806, 2013. Statistical analysis indicated a good quality of the thermal adjustment, with the exception of Prot. 3 with rear air camera, which exhibited uncertain adequacy of the

numerical model applied. Further study is recommended for this case. For the rest of cases, optical efficiency and heat loss coefficients were calculated with good statistical indicators, which enables the estimation of the thermal and electrical power productions at certain external conditions (solar irradiance, ambient temperature and wind speed). This approach has been then used to determine their potential at the required operational temperature (above 50ºC).

From the prototypes proposed, two PVT models without frontal cover (unglazed collector with high performance PV laminate and collector with intermediate camera with semi-transparent PV laminate) showed low thermal efficiency for the required operational temperature. Particularly, unglazed case presented the highest electrical performance (around 19%) but really low thermal generation (105 W/m^2) at high temperatures, which dismisses its use for this application but remain for others where lower temperatures or more electrical efficiency are sought. On the other hand, the other two prototypes exhibited acceptable thermal productions at 50ºC. Both prototypes include a frontal cover that minimizes the heat losses on the collector. As a consequence, they reach to produce up to 314 W/m^2 (Prot. 2 with full PV laminate) and 481 W/m^2 (Prot. 4 with semi-transparent PV laminate). The difference between them remains also in the electrical production, with greater values for the case of full laminate rather than semi-transparent PV laminate, up to 70% higher.

Results indicate that the incorporation of semi-transparent PV laminate may help to improve the thermal performance of the glazed PVT collectors, especially when working at high temperatures (around 25ºC above environment, as required for this project). However, it reduces the electrical production, so their use should be reserved for applications where thermal contribution is crucial.

5. Acknowledgments

6. References

Baggenstos, A., Mellor, A., Gagliano, A., Corino, C., Zenhäusern, D., Cabral, D., Ryan, G., Guedea, I., Brottier, L., Ruoff, U., Schubert, M., Lämmle, M., Pellegrini, M., Dannemand, M., Cañada, M., Radish, N., Pokorny, N., Ramshack, T., 2020. Existing PVT systems and solutions. IEA SHC Task60, PVT Systems, Report A1, 1st ed. https://doi.org/10.18777/ieashc-task60-2020-0001

Bianchini, A., Guzzini, A., Pellegrini, M., Saccani, C., 2017. Photovoltaic/thermal (PV/T) solar system: Experimental measurements, performance analysis and economic assessment. Renew. Energy 111, 543–555. https://doi.org/10.1016/j.renene.2017.04.051

Brötje, S., Kirchner, M., Giovannetti, F., 2018. Performance and heat transfer analysis of uncovered photovoltaic-thermal collectors with detachable compound. Sol. Energy 170, 406–418. https://doi.org/10.1016/j.solener.2018.05.030

Fayaz, H., Rahim, N.A., Hasanuzzaman, M., Rivai, A., Nasrin, R., 2019. Numerical and outdoor real time experimental investigation of performance of PCM based PVT system. Sol. Energy 179, 135–150. https://doi.org/10.1016/j.solener.2018.12.057

Herez, A., El Hage, H., Lemenand, T., Ramadan, M., Khaled, M., 2020. Review on photovoltaic/thermal hybrid solar collectors: Classifications, applications and new systems. Sol. Energy 207, 1321–1347. https://doi.org/10.1016/j.solener.2020.07.062

IEA-SHC, 2022. Solar Thermal Market Records Year of Growth, Solar update. The Newsletter of the IEA Solar-Heating and Cooling Programme. USA.

IEA-SHC, 2018. Task 60 - PVT Systems: Application of PVT Collectors [WWW Document]. URL https://task60.iea-shc.org/

ISO 9806, 2017. Solar energy - Solar thermal collectors - Test methods. Second Edition.

ISO 9806, 2013. ISO 9806:2013 Solar energy - Solar thermal collectors - Test methods.

Jonas, D., Lämmle, M., Theis, D., Schneider, S., Frey, G., 2019. Performance modeling of PVT collectors: Implementation, validation and parameter identification approach using TRNSYS. Sol. Energy 193, 51–64. https://doi.org/10.1016/j.solener.2019.09.047

Joshi, S.S., Dhoble, A.S., 2018. Photovoltaic -Thermal systems (PVT): Technology review and future trends. Renew. Sustain. Energy Rev. 92, 848–882. https://doi.org/10.1016/j.rser.2018.04.067

Ozgoren, M., Aksoy, M.H., Bakir, C., Dogan, S., 2013. Experimental performance investigation of photovoltaic/thermal (PV-T) system, in: European Physical Journal Conferences. https://doi.org/10.1051/epjconf/20134501106

Simón-Allué, R., Guedea, I., Coca-Ortegón, A., Villén, R., Brun, G., 2022. Performance evaluation of PVT panel with phase change material: Experimental study in lab testing and field measurement. Sol. Energy 241, 738–751. https://doi.org/10.1016/j.solener.2022.05.035

Sultan, S.M., Ervina Efzan, M.N., 2018. Review on recent Photovoltaic/Thermal (PV/T) technology advances and applications. Sol. Energy 173, 939–954. https://doi.org/10.1016/j.solener.2018.08.032

Wu, J., Zhang, X., Shen, J., Wu, Y., Connelly, K., Yang, T., Tang, L., Xiao, M., Wei, Y., Jiang, K., Chen, C., Xu, P., Wang, H., 2017. A review of thermal absorbers and their integration methods for the combined solar photovoltaic/thermal (PV/T) modules. Renew. Sustain. Energy Rev. 75, 839–854. https://doi.org/10.1016/j.rser.2016.11.063

Zisopoulos, G., Nesiadis, A., Atsonios, K., Nikolopoulos, N., Stitou, D., Coca-Ortegón, A., 2021. Conceptual design and dynamic simulation of an integrated solar driven thermal system with thermochemical energy storage for heating and cooling. J. Energy Storage 41. https://doi.org/10.1016/j.est.2021.102870